Experimental Observation and Constitutive Equations of Fracture Propagation

Alexander Chudnovsky[1], Zhenwen Zhou[1], Haiying Zhang[1,*]

[1] Department of Civil and Materials Engineering, University of Illinois at Chicago, 60607, USA
* Corresponding author: haiyin@uic.edu

Abstract There is a long list of empirical slow crack growth (SCG) equations that present the crack propagation rate as a function of stress intensity factor (SIF) or energy release rate (ERR). Experiments with crack growth through a heterogeneous stress field reveal the limitations of such type of equations resulting from existence of a process zone (PZ) surrounding the crack. PZ is a material "defense" against stress concentration caused by the crack and is commonly observed in most of engineering materials. It plays an important role in determination of the direction and rate of fracture propagation. Therefore, the PZ and crack are treated as two coupled elements of one Crack Layer (CL) system and CL propagation is represented by two coupled possesses: (i) the PZ evolution by transformation of the original material into a "damaged" and often anisotropic PZ material and (ii) crack growth into PZ. The CL driving forces are introduced as the negative derivative of Gibbs free energy with respect to CL geometrical parameters. The constitutive equations of CL propagation are formulated in form of simple relations between the crack and PZ growth rates and corresponding thermodynamic forces. Qualitative analysis of these equations suggests two distinctly different patterns of CL propagation: continuous and discontinuous, stepwise growth. A special experimental setup and test material have been selected to simplify and examine the proposed constitutive equations of CL growth. CL model provides a very good agreement with a large set of experimental data at various load levels, temperatures and specimen geometries.

Keywords Crack layer model, slow crack growth, process zone, constitutive equations

1. Introduction

Crack in engineering materials formed under fatigue and creep conditions usually appears as a narrow cut with small amplitude random deviations from a straight or slightly curved trajectory. A close observation of such crack reveals a presence of a process zone (PZ) (also called damage zone, plastic deformation zone, etc.) that precedes and surrounds the crack. Depending on material chemical composition and morphology, temperature, loading rate, specimen geometry, etc. various types of micro defects such as crazes, shear bands, microcracks, micro-voids constitute PZ. In general, micro-defects are strain localizations on micro scale and based on their orientation one can distinguish brittle, such as crazes and micro-cracks, and ductile like shear bands and micro-voids, types of damage. The micro-defects are commonly formed in response to stress concentration, and shield the vicinity of the crack front from high elastic stresses by increase of an effective (inelastic) material compliance. The crack growth is closely coupled with formation and evolution of the micro-defects population within PZ. A system of coupled crack and PZ is referred to as Crack Layer (CL).

There is a strong interaction between micro-defects in a vicinity of the crack front and the crack [1–4]. It results in significant modification of the crack tip fields. Apparently, it also affects the stress intensity factor (SIF) K. Figure 1 illustrates the effect of micro-cracking (displacement discontinuities) on SIF. An individual micro-crack is modeled as a displacement discontinuity across an elementary segment (area in 3D) with orientation $\underline{n}$ and displacement jump $\underline{b}$. In the specific example shown in Figure 1 all micro-cracks are considered to be parallel to the crack and have opening in the normal direction. The arrays of curves emanating from the crack tip forward and backward present contours of equal level of the mode I SIF Green's function $G_1^{SIF}(\underline{\xi})$ due to unit normal displacement dipole with $\underline{n}(0,1)$ and $\underline{b}(0,1)$ at the point $\underline{\xi}$ [3–5]. The continuous lines indicate SIF amplification effect due to the discontinuities located on the lines in front of the crack; whereas the two "butterfly wings" of dotted lines show the reduction of SIF, i.e., shielding effect of the discontinuities located on the lines

on both sides of the crack. The numbers above the lines indicate the magnitude of amplification and reduction of SIF. The external solid line indicates schematically the boundary of the process zone and therefore CL.

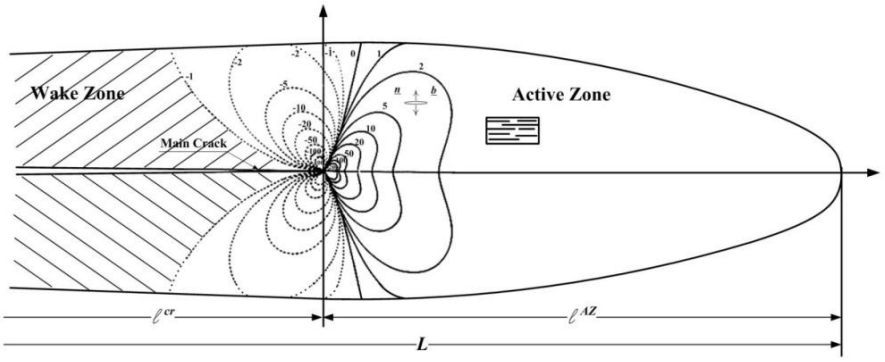

Figure 1. Dimensionless Mode-I SIF Green's Function due to a unit normal displacement dipole with orientation (θ = 0°) with respect to the x-axis.

By distributing the individual micro-cracks and passing to a continuum damage, we introduce damage density as a bivector $\rho(\underline{\xi})$ that represents the total micro-cracks area per unit volume (with dimensions $[\rho] = mm^2/mm^3$). There is a domain of PZ, where the defects constituting PZ strongly interact with crack by shielding and/or amplifying the crack tip fields. The crack in turn causes the new defects formation and growth, i.e., $\dot{\rho} \geq 0$ in that domain. Such domain is referred to as active zone (AZ) of CL. It leads to material degradation in the immediate vicinity of crack front and crack movement into PZ. As the crack advances through AZ, the latter "moves" away from the crack by forming new defects and leaves behind a wake zone (WZ) constituted by the defects that remain after unloading of AZ. Thus, CL propagation occurs as AZ "movement" in material frame of reference and crack advancement into AZ.

The total SIF is the sum of SIF K_I^0 due to remote load and the increment of SIF due to distributed micro-cracks with opening $\underline{b}$ dependent on the main crack – micro-cracks array interaction [3–5]:

$$K_I^{tot} = K_I^0 + \int_V G_I^{SIF}(\xi_i) \cdot b(\xi_i) \wedge \rho(\xi_i) dV \,. \tag{1}$$

The calculations suggest that the shielding effect (a negative SIF increment) is stronger than the amplification and the total SIF in some cases is vanishing [4]. In such cases the "beak" type crack tip opening displacement profile is observed [1].

2. Experimental and Results

To observe the details of CL evolution a set of creep tests was conducted at various loads and temperatures. The creep testing machine equipped with high temperature chamber with four creep stations and two observation windows, pneumatic system of graduate load application and continuous displacement monitoring device is used for tests (see Figure 3 (a)).

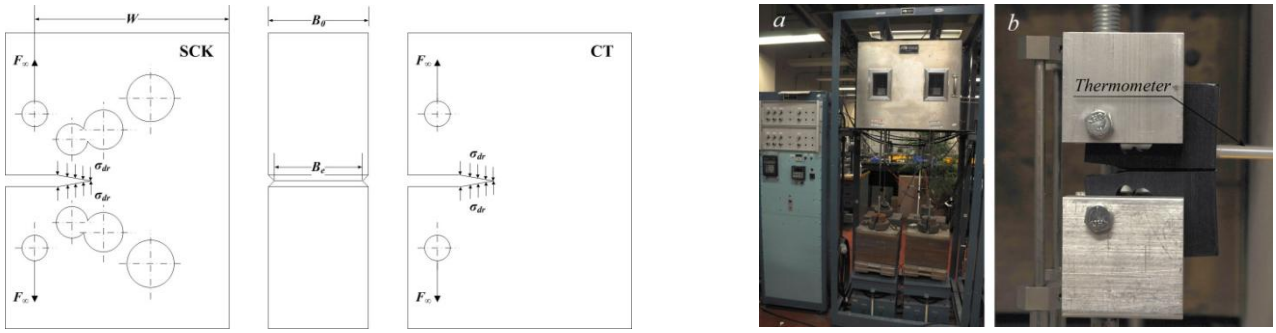

(b) (a)

Figure 3. (b) The geometry and loading of SCK and CT specimens; (a) Slow crack growth test setup.

Various specimen geometries have been used in the tests. One is the standard compact tension (CT) specimen. Another is a specially design stiff constant-*K* (SCK) specimen. SCK specimen poses the highest stiffness among comparable specimen geometries and provides a constant *K* within the crack size range $0.15 < a/W < 0.4$. The diameters and locations of holes are designed to maintain the constancy of SIF while crack is propagating. The side grooves are introduced to reduce the plane stress effect within the surface layers and guide the crack growth along the plane of symmetry. The CT specimen has the same shape and dimension as that in SCK, but does not have holes, as shown in Figure 3 (b). Both types CT and SCK specimens were machined from a commercial large diameter HDPE pipe with $3''$ wall thickness. The SIF is continuously increasing with crack growth in CT specimen. We selected HDPE material for this study since it displays the simplest, but not trivial PZ geometry observable in fracture experiments: a narrow wage shape domain of cold drawn fibers and membranes with sharp boundaries separating PZ and original bulk material.

Figure 4 shows the records of the load-point displacement vs. time monitored in the creep tests at various loads (SIFs) and temperatures. Curve *a* in Figure 4 (initial SIF: $K_0 = 10MPa \cdot \sqrt{mm}$ and $T = 80^{o}\mathrm{C}$) clearly shows a transition from continuous to stepwise growth. The same but subtler transition is also observed in Curve *b* (initial SIF $K_0 = 12MPa \cdot \sqrt{mm}$ and the same temperature compared to Curve *a*). At the same temperature, if the SIF is increased to $K_0 = 18MPa \cdot \sqrt{mm}$ (initial SIF), a pure stepwise growth is observed as displayed by Curve *c*. The length of individual step in CT specimen is continuously increasing due to the increasing SIF in contrast with that in SCK specimen (reported in [6]). However, there are no visible steps in load-point displacement record (Curve *d*), even for a significantly higher load ($K_0 = 48MPa \cdot \sqrt{mm}$ initial SIF), if the temperature is reduced to room temperature ($T = 23^{o}\mathrm{C}$),.

The continuous, discontinuous as well as transitional mechanisms of SCG are revealed even more explicitly by CL side view and fracture surfaces. For example, a homogeneous and continuous CL growth occurs at an elevated temperature with a much lower initial SIF ($K_0 = 10MPa \cdot \sqrt{mm}$) (see Figure 5 (a)). The upper picture in Figure 5 (a) presents a general view of CL developed during 290 hours of creep with initial SIF $K_0 = 10MPa \cdot \sqrt{mm}$ at 80°C. There are no steps as well, rather monotonically decreasing width of the triangular CL and crack opening toward a very weakly visible PZ tip. The bottom picture shows a homogeneous surface without any striations. At the very end, we can see a smooth strip that corresponds to the last process zone broken in liquid nitrogen.

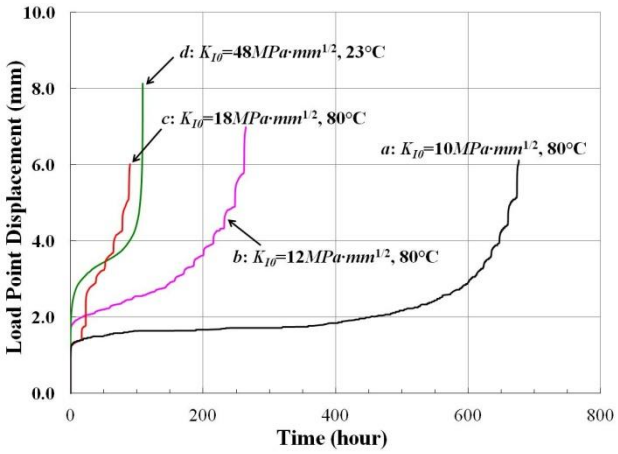

Figure 4. Load-point displacement vs. time recorded in creep test conducted at *a*) $K_0 = 10MPa \cdot \sqrt{mm}$, $T = 80^{\circ}\mathrm{C}$; *b*) $K_0 = 12MPa \cdot \sqrt{mm}$, $T = 80^{\circ}\mathrm{C}$; *c*) $K_0 = 18MPa \cdot \sqrt{mm}$, $T = 80^{\circ}\mathrm{C}$; *d*) $K_0 = 48MPa \cdot \sqrt{mm}$, $T = 23^{\circ}\mathrm{C}$.

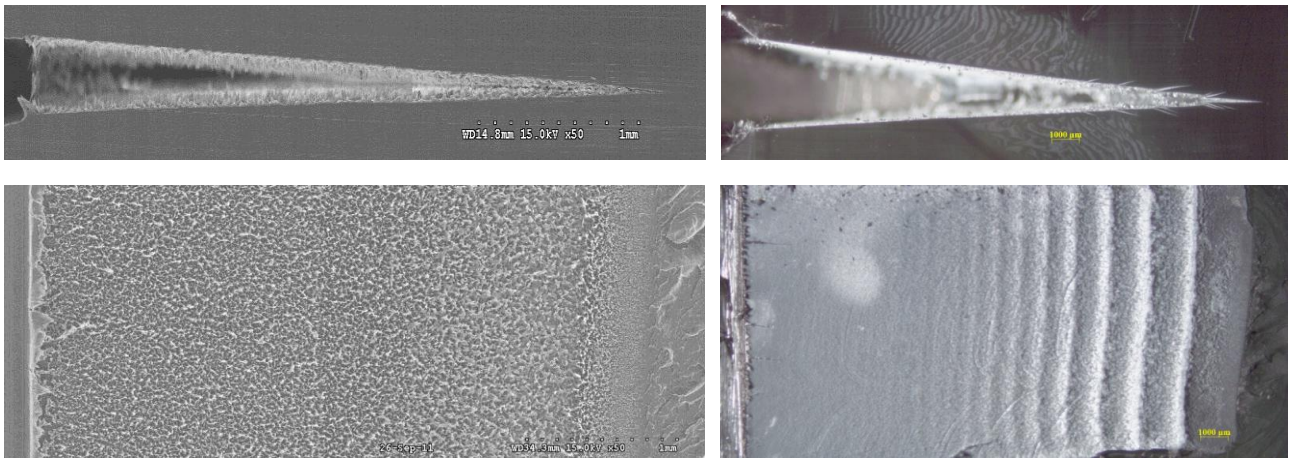

(a) (b)

Figure 5. CT specimens tested at 80°C with initial $K_0 = 10MPa \cdot \sqrt{mm}$: (a) tested for 290 hours, Upper: side view; Lower: fracture surface. (b) tested for 680 hours, Upper: side view; Lower: fracture surface.

The striking observation is that, given the same testing conditions ($K_0 = 10MPa \cdot \sqrt{mm}$, 80°C), if the test is conducted longer (680 hours), a transition from continuous to stepwise growth occurs. The upper picture in Figure 5 (b) depicts a monotonically decreasing opening of crack toward the tip, and pairs of symmetrical "flankers" emanating from two sides of the boundary in the region close to the crack tip. The positions of flankers correspond to white shining striations observed in the lower image, and are signs of discontinuous growth. This evolution from continuous to stepwise growth is manifested in the lower image in such a way that fracture surface first shows homogeneity then striations gradually appear with a wider and wider spacing due to increasing SIFs.

When the initial SIF is increased to certain level, the discontinuous fracture propagation takes place from the beginning. It is illustrated in Figure 6 that shows CL in a CT specimen tested at 80°C with initial SIF $K_0 = 18MPa \cdot \sqrt{mm}$ (Note: the sample was step loaded from $K = 12MPa \cdot \sqrt{mm}$ to $K = 18MPa \cdot \sqrt{mm}$ during a short period, and the latter is considered as the initial SIF.). A wedge-type pulsating domain indicates a discontinuously CL grown with six well defined steps in upper image

(the very first step is neglected for reason addressed above). Five steps are filled with drawn and broken fibers. The sixth one, a weakly visible and elongated wedge type domain, is the process zone with freshly drawn intact fibers. The fibrillated process zone is separated by a sharp boundary from a uniform grey domain of the original HDPE. It is also obvious that five completed steps exhibit an increasing size of PZ, in contrast with an equal size PZ in SCK specimen [6].

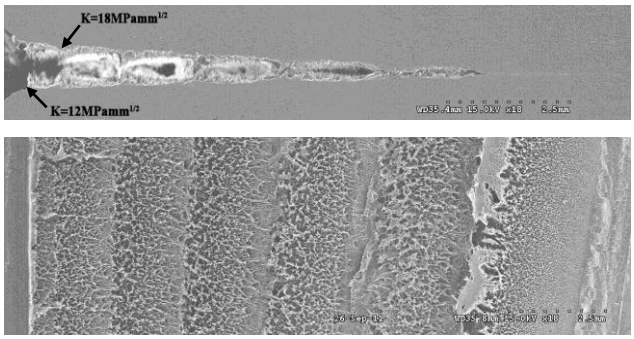

Figure 6. CL in CT specimen tested at 80°C with an initial SIF $K_0 = 18MPa \cdot \sqrt{mm}$ for 90 hours, Upper: side view; Lower: fracture surface (18×).

The data presented above clearly indicate that there are two different mechanisms of SCG: continuous and discontinuous ones. The transition from continuous to discontinuous SCG strongly depends on stress and temperature. A SCG mechanisms map has been proposed and discussed in [6, 7]. The equilibrium process-zone sizes are recorded using micrographs similar to that shown in Fig.6 and used for evaluation of CL parameters. Details of such work are presented in the accompanying paper [8].

3. Constitutive Equations of CL Model

As stated above, CL in PE poses the simplest PZ that displays the characteristic features of PZ evolution. Therefore, we use it as a showcase for formulation of CL constitutive equations.

3.1. Crack Layer Thermodynamic Forces

The active zone of CL in PE has narrow wedge shape geometry with a sharp boundary separating PZ from the surrounding original material (see upper Fig.5a). It consists of cold drawn fibers connected with original material. The crack propagation is the process of breaking fibers under creep condition and forming a fracture "surfaces" (see lower Fig 5a). The width of CL is very small in comparison to the CL length. Therefore we employ the conventional Fracture Mechanics formalism in modeling the external with respect to CL domain. However, addressing the fracture propagation through AZ we use an effective continuum with properties reflecting discrete fibrillated and oriented AZ material. In energy balance, we also consider the energy of transformation of the original material into cold drawn, highly oriented structure of PZ. For such analysis, it is convenient to decompose the specimen with CL into a specimen with CL cutoff and a thin wedge shape CL domain with variable width ω_0 of original material that undergoes cold drawing in process of PZ formation (see Figure 8). The stress analysis problem shown in Figure 8 (a) is presented as superposition of the same specimen geometry and external load with a cut of CL. The mechanical interaction between AZ of CL and the specimen is taken into consideration by application of the drawing stress σ_{dr} along the boundaryof AZ since there is a mechanical equilibrium between the drawn and original materials along that boundary (see Figure 8,b). The second part of the superposition is CL cutoff with stress σ_{dr} acting on the AZ from the specimen side (Figure 8,c). The width of AZ in the reference configuration ω_0 is a function of

location x, $0 \le x \le \ell^{AZ}$ within AZ and time t, since AZ evolves in time: $\omega_0 = \omega_0(x,t)$. Fig 8a should be AZ instead of PZ

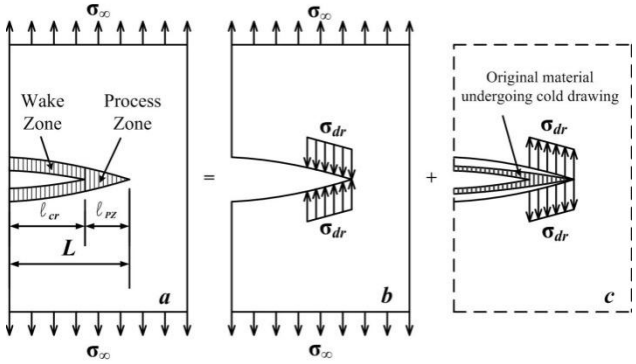

Figure 8. Decomposition of the stress analysis problem of CL

The width of AZ in actual configuration (after drawing) is $\omega = \lambda \cdot \omega_0$ (λ is the natural draw ratio). Thus, the displacement discontinuity in normal to the crack direction due to cold drawing is $(\lambda - 1)\omega_0$. To determine the amount of material that undergoes cold drawing and builds up AZ, i.e., the width ω_0, we consider crack opening displacement (COD) as an approximation of the opening of a slit in the specimen with CL cutoff. The approximation is quite accurate due to presence of a small parameter: the ratio of the width over the length of the slit. Then, we make use of conventional Fracture Mechanics formalism and compute COD for the boundary value problem depicted in the Figure 8b. Thus, ω_0 is found from the continuity conditions of the original problem: the COD $\delta(x, t)$ in the specimen with PZ cutoff and the traction σ_{dr} along AZ boundary should be equal to the displacement discontinuity in drawing process within AZ:

$$\omega_o(x,t) = (\lambda - 1)^{-1} \cdot \delta(x,t)\,. \tag{2}$$

The Eq. (2) establishes the functional relation between the width ω_0 and COD in the specimen and loading shown in the Figure 8b. The COD depends on applied load σ_∞, σ_{dr} and the specimen dimensions W, crack length ℓ^{cr}, AZ length ℓ^{AZ} and CL lengths L ($L = \ell^{cr} + \ell^{AZ}$). Thus, in this case, we have only two independent geometrical parameters of CL (ℓ^{cr} and ℓ^{AZ}), since ω_0 is not an independent one. That is the reason for simplification of CL in PE: it is reduced to two-parameter model. The stationary state of a solid with two-parameter CL is determined by the minimum of the total Gibbs potential G_{tot} for the problem of Fig 8a. Based on the decomposition of Fig. 8, the total Gibbs potential is the sum of the Gibbs potentials of the specimen with CL cutoff G_0 and the PZ potential G_{PZ} illustrated in Figure 8:

$$G_{tot} = G_0(\sigma_\infty, T, \sigma_{dr}; L, \ell^{AZ}, W) + G_{PZ}(\sigma_{dr}; \ell^{cr}, \ell^{AZ}, T)\,. \tag{3}$$

The Gibbs potential of PZ in turn consists of the wake zone G_{WZ} and active zone G_{AZ} potentials (see the definitions on WZ in Figure 1). AZ consists of homogeneous drawn material with properties different from that of the surrounding original material. It is also separated from the original by distinct boundary with drawing stress acting along it. As a result, the AZ Gibbs potential can be presented as:

$$G_{AZ} = \gamma^{tr} \cdot V_{AZ}\,. \tag{4}$$

The multiplier γ^{tr} in Eq. (4) stands for the specific energy of transformation of a unit mass of original material into the oriented drawn state under drawing stress σ_{dr}: $\gamma^{tr} = g^{tr}(T) - g^0(T)$, where the Gibb potential density is defined as $g(\sigma,T) = f(\varepsilon,T) - w$, where $f(\varepsilon,T)$ is the strain energy density and w stands for work density [9].

The potential of WZ is different in two ways: 1) it does not contain the strain energy of the stretched

fibers, since the crack is traction free; and 2) it contains the surface energy term of the crack faces:

$$G_{WZ} = \gamma_0^{tr} \cdot V_{PZ} + \gamma \cdot \ell^{cr} . \tag{5}$$

Finally, the total Gibbs potential can be expressed as follows:

$$G_{tot} = G_0(\sigma_\infty, \sigma_{dr}; L, \ell^{AZ}, W) + \gamma^{tr} \cdot V_{AZ}(\sigma_{dr}; \ell^{cr}, \ell^{AZ}) + \gamma_0^{tr} \cdot V_{WZ}(\ell^{cr}, L) + \gamma \cdot \ell^{cr} . \tag{6}$$

We compute the volume V^{AZ} of AZ material in the reference state by integrating the AZ width, which is expressed in terms of total COD in the specimen with PZ cutoff (Eq. (2)):

$$V^{AZ} = B_{eff} \int_{\ell^{cr}}^{L} \omega_o(x) dx = \frac{B_{eff}}{\lambda - 1} \int_{\ell^{cr}}^{L} \delta_{tot}\left(x; \ell^{cr}, \ell^{AZ}, W; \sigma_\infty, \sigma_{dr}\right) dx . \tag{7}$$

The total COD δ_{tot} in Eq. (7) is obtained as the superposition of COD $\delta_\infty = \delta_\infty(\sigma_\infty, L)$ due to remote load σ_∞ and crack "closure" $\delta_{dr} = \delta_{dr}(\sigma_{dr}; \ell^{cr}, \ell^{AZ})$ by the traction σ_{dr} acting along AZ boundary as shown in Figure 8.

The thermodynamic forces X^{AZ} and X^{CR} responsible for AZ (ℓ^{AZ}) and crack (ℓ^{cr}) growth are expressed as the partial derivative of total Gibbs potential G_{tot} with respect to corresponding parameters ℓ^{cr} and ℓ^{AZ}, since they are the only independent geometrical characteristics of CL:

$$X^{CR} = -\frac{\partial G_{tot}}{B_{eff} \partial \ell^{cr}}; \qquad X^{AZ} = -\frac{\partial G_{tot}}{B_{eff} \partial \ell^{AZ}} . \tag{8}$$

The derivative with respect to crack length ℓ^{cr} of the first term of G_{tot} decomposition Eq. (6) is zero, when CL length L is fixed. The derivative of the second and third terms of Eq. (6) is the energy release rate (ERR) J_1^{cr} due to crack extension into PZ, when PZ is stationary (L is constant); and the derivative of the fourth term is simply 2γ. Thus, the thermodynamic force reciprocal to crack length is:

$$X^{CR} = J_1^{cr} - 2\gamma . \tag{9}$$

We compute the thermodynamic force reciprocal to AZ in a similar manner considering the specimen with PZ cutoff as a linear elastic solid. The derivative of the first term of decomposition Eq. (6) gives the energy release rate in the specimen with crack of length L loaded by remote load σ_∞ and traction σ_{dr} applied on ℓ^{AZ} part of L:

$$-\frac{\partial G_0}{B_{eff} \partial \ell^{AZ}} = G_1 = \frac{K_{tot}^2}{E'} , \tag{10}$$

where E' is the plain strain Young's modulus and K_{tot} is the sum of SIFs due to remote load and traction along the AZ boundary:

$$K_{tot} = K_\infty(\sigma_\infty, L, W) - K_{dr}(\sigma_{dr}, W, L, \ell^{AZ}) , \tag{11}$$

The derivative of the V^{AZ} (Eq. (7)) with respect to ℓ^{AZ} is expressed as the following integral:

$$\frac{\partial V^{AZ}}{B_{eff} \partial \ell^{AZ}} = \frac{1}{\lambda - 1} \int_{\ell^{cr}}^{L} \frac{\partial \delta_{tot}}{\partial \ell^{AZ}}\left(x; \ell^{cr}, \ell^{AZ}, W; F_\infty, \sigma_{dr}\right) dx . \tag{12}$$

It is evaluated numerically and found to be approximately equal to COD at the root of PZ with a reasonable accuracy (any estimation of accuracy?):

$$\frac{\partial V^{AZ}}{B_{eff}\partial \ell^{AZ}} \cong \left.\frac{\delta_{tot}\left(x;\ell^{cr},\ell^{AZ},L,W;F_{\infty},\sigma_{dr}\right)}{\lambda-1}\right|_{x=\ell^{cr}}. \tag{13}$$

Since the WZ does not change if ℓ^{cr} is fixed, the derivative of the third term in Eq. (6) with respect to ℓ^{AZ} is zero. Finally, putting together Eq. (6), Eq. (8), Eq. (10) and Eq. (13) we obtain the expression for X^{AZ}:

$$X^{AZ} = \frac{K_{tot}^2}{E'} - \left.\frac{\gamma^{tr}}{\lambda-1}\cdot\delta_{tot}(x)\right|_{x=\ell^{cr}}. \tag{14}$$

The AZ reaches equilibrium when the thermodynamic force is vanishing. Therefore, the equilibrium AZ length ℓ_{eq}^{AZ} is determined by the following equation:

$$\frac{K_{tot}^2}{E'} - \left.\frac{\gamma^{tr}}{\lambda-1}\cdot\delta_{tot}(x)\right|_{x=\ell^{cr}} = 0. \tag{15}$$

For a given external load, and crack length, the equilibrium AZ size depends on γ^{tr} and drawing stress σ_{dr}. The cold drawing phenomenon in PE is long studied using macroscopical specimens. It is well established that the drawing stress σ_{dr} increases with the loading rate [7]. Unfortunately, it is difficult to evaluate σ_{dr} on microfibers. Therefore, we use the linear relations between σ_{dr} and log strain rate obtained in macroscopical tests. Since the loading rate of the AZ material changes with CL growth, the σ_{dr} acting along AZ boundary is also varies with CL growth and can be estimated on the basis of either a combination of COD rate and macroscopical $\sigma_{dr}\sim\ln\dot{\varepsilon}$ relations or indirectly on duration of AZ stationary state. Regarding γ^{tr}, the transformation of the original continuum media into highly oriented fibrillated structure within PZ is a complex process. It starts with cavitation ahead of the crack front as a precursor of drawing. The cavitation makes it possible to draw thin membranes between the cavities. Further drawing leads to splitting some of the membranes into thin fibers. For such micron scale of processes, a surface energy of microfibers and membrane becomes comparable to the bulk material energy. It complicates a theoretical evaluation of γ^{tr}. A comparison of the value of AZ size ℓ_{eq}^{AZ} resulting from solution of the Eq. (16) with actual ℓ_{eq}^{AZ} observed in the experiment allows evaluating of an effective (phenomenological) value of γ^{tr}. This estimation has been performed and reported in a separate paper accompanying this one.

3.2. Kinetic Equations of Crack Layer Growth in PE

A stationary CL configuration takes place, when the CL thermodynamic forces are not positive, i.e., $X^{AZ}\le 0$ and $X^{CR}\le 0$. The equilibrium is achieved, when the forces equal 0 (for example Eq. (15) for AZ equilibrium). At a small deviation from equilibrium, a thermodynamic system has a tendency to return to the equilibrium state. However, fracture is an essentially irreversible process: there is no return, when the crack is moving into AZ by breaking fibers, or AZ advances into the original material via cavitation followed by cold drawing of the material between the cavities and formation of membranes and fibers. Thus, when CL departs from equilibrium stationary state, it evolves to the next stationary configuration.

Close observation of the micromechanisms of CL growth reveals that there is always formation of AZ first in a vicinity of a a micro defect or specially made notch. After some time of growth, AZ reaches a stationary state, at which its length does not visibly change. It implies that the thermodynamic force reciprocal to AZ length has vanished. During that time, however, we observe an increasing load point displacement. It can be noticed from the load point displacement records of discontinuous (stepwise) SCG (Figure 4). The increase of load point displacement during a stationary AZ size stems from the macroscopical creep of the bulk material accompanied by an increasing width of AZ. The later may result from either drawing of an additional material across AZ boundary or creep of the drawn material of AZ or both.

The absence of a crack growth from a macroscopical view point means that the crack driving force $X^{CR} \leq 0$, i.e., $J_1^{CR} \leq 2\gamma$. This inequality may change the sign after a certain time of creep and degradation of fibers within AZ, since the specific fracture energy γ decays due to degradation of microfibers. Then, the crack moves into AZ for the distance controlled by an interplay between J_1^{CR} and $2\gamma(x,t)$. The advancement of the crack into AZ reduces AZ length and thus violates the AZ equilibrium condition, giving rise to an increase of AZ force that result in the AZ growth.

Thus, the role of AZ is in moderating high stress concentration caused by a crack. It is achieved by strain localization (displacement discontinuity) in form of cavitation and cold drawing. However, AZ can only delay the fracture propagation process: the creep and/or other types of degradation of the AZ material reduce its toughness with time and ultimately allow crack penetration into AZ. Such process of CL propagation continues by crack and AZ assisting mutual growth. The described scenarios of CL growth is formalized in the following system of coupled ordinary differential equations with respect to ℓ^{cr} and ℓ^{AZ}:

$$\begin{cases} \dot{\ell}^{cr} = k_1 X^{CR}, & if\ X^{CR} \geq 0,\ and\ \dot{\ell}^{cr} = 0,\ if\ X^{CR} < 0 \\ \dot{\ell}^{AZ} = k_2 X^{AZ}, & if\ X^{AZ} \geq 0,\ and\ \dot{\ell}^{AZ} = 0,\ if\ X^{AZ} < 0 \end{cases}. \tag{16}$$

The kinetic coefficients k_1 and k_2 in Eq. (16) as well as the parameters entering the CL driving forces X^{AZ} and X^{CR} are evaluated by matching the model predictions with observed CL evolution reflected by load point displacement vs. time plot like shown in Figure 4, side views and fracture surface micrographs similar to that shown in Figures 5, 6, and 7.

The crack and AZ thermodynamic forces are non-linear functions of crack and AZ lengths. Thus, the system of Eq. (17) despite of its simple appearance is a nonlinear system of ODE, solution of which calls for numerical methods. An illustration of numerical simulation of CL growth in a CT specimen is presented in the accompanying paper [8].

4. Conclusion

The focus of the paper is brittle fracture resulting from SCG. The limitation of the conventional approach of lifetime assessment in brittle fracture originates from complexity of SCG process. Specifically, relatively new data on continuous vs. discontinuous modes of SCG is presented in details. Only continuous CL growth takes place for low enough load. Above that value, both continuous and discontinuous modes of SCG are possible at different temperature.

The active zone of CL constituted by cold drawn microfibers and the energy dissipation associated with AZ formation play a major role in fracture process. A brittle fracture of microfibers in process

of drawing or soon after completion of drawing results in a continuous CL growth. In contrast with that, a ductile behavior (creep) of drawn microfibers within AZ is the underlying cause of the discontinuous CL growth.

A transition in the mechanism and kinetics of SCG takes place at certain combination of temperature and SIF. It suggests that commonly used extrapolation of data obtained at elevated temperature into service condition is limited by the requirement of similarity in the mechanisms and kinetics of fracture process. Therefore, the commonly used acceleration technique based on extrapolation of 1-1.5 years elevated temperature test data into 50 and 100-year life in service condition is a suspect. In addition, there is a hidden assumption that after decades of services the material retains the same properties as the one tested for a year or two. The material aging process (chemical degradation and/or physical aging) commonly takes place over time. It should be taken into consideration. An alternative approach to the lifetime assessment problem is a formulation of a sound physical model of initiation and SCG processes and numerical simulation of brittle fracture.

References

[1] A. Chudnovsky, Experimental and theoretical studies of slow crack growth in engineering polymers, Key Eng Mat, 345 (2007) 493–496.
[2] A. Chudnovsky, A. Dolgopolsky and M. Kachanov: Elastic interaction of a crack with a microcrack array—I. Formulation of the problem and general form of the solution, Int J Solids Struct, 23 (1987) 1–10.
[3] A. Chudnovsky, A. Dolgopolsky and M. Kachanov: Elastic interaction of a crack with a microcrack array—II. Elastic solution for two crack configurations (piecewise constant and linear approximations), Int J Solids Struct, 23 (1987) 11–21.
[4] M. Ben Ouezdou and A. Chudnovsky, Semi-empirical crack tip analysis, Int J Fracture, 37 (1988) 3–11.
[5] S. Wu and A. Chudnovsky, A., Elastic interaction of a crack with a random array of microcracks, Int J Fracture, 49 (1991) 123–140.
[6] Z. Zhou, H. Zhang and A. Chudnovsky, Temperature effects on slow crack growth in pipe grade PE, Proceedings of the 68th Annual Technical Conference & Exhibition, ANTEC 2010, Society of Plastics Engineers, Orlando, FL, 2010, pp. 679–684.
[7] A. Chudnovsky, Z. Zhou, and H. Zhang, Lifetime Assessment of Engineering Thermoplastics, Int J Eng Sci, 59 (2012) 108–139.
[8] H. Zhang, Z. Zhou and A. Chudnovsky, Computational Method for CL Model, …
[9] J. D. Eshelby, Energy relations and the energy-momentum tensor in continuum mechanics, in: M. F. Kannien, W. F. Adler, A. R. Rosenfeld, and R. I. Taffee (Eds.), Inelastic Behavior of Solids, McGraw-Hill, New York, 1970, pp. 77–115.